Linear and nonlinear optical properties of gold nanospheres immobilized on a metallic surface

Shinya Abe[1] and Kotaro Kajikawa[1,2,*]

[1]*Interdisciplinary Graduate School of Science and Engineering, Tokyo Institute of Technology, Nagatsuta, Midori-ku, Yokohama 226-8502, Japan*

[2]*PRESTO, Japan Science and Technology Agency, 4-1-8 Honcho, Kawaguchi, Saitama 332-0012, Japan*

(Received 14 December 2005; revised manuscript received 30 March 2006; published 14 July 2006)

We studied linear and nonlinear optical properties of surface-immobilized gold nanospheres (SIGNs) above a metallic surface with a gap distance of a few nanometers. The nanogap is supported by self-assembled monolayers (SAMs); they are used as spacers. A localized surface plasmon resonance (LPR) band ($\lambda = 600-700$ nm) redshifted from the LPR band of isolated gold nanospheres ($\lambda \sim 520$ nm) is observed in the *p*-polarized reflection absorption spectra with oblique incidence. This band originates from the electromagnetic interaction of the gold nanospheres with their images produced in the metallic substrate. The amount of redshift depends on the gap distance, which is controlled by the thickness of the SAMs. These optical properties can be simulated using theoretical calculations obtained by considering multipolar interactions based on a quasistatic approximation. Further, in SIGNs above a metal, we observed a significantly enhanced optical second-harmonic generation (SHG). The field enhancement factor was found to be greater than 10 at 1064 nm. This is due to an increase in local electric fields in SIGN systems at both fundamental and SHG wavelengths ($\lambda^{2\omega} = 532$ nm). Local electric field calculations imply that the SHG from the nanogap does not dominate even under the LPR condition because the nanogap region is almost centrosymmetrical.

DOI: 10.1103/PhysRevB.74.035416 PACS number(s): 78.67.Bf, 42.65.−k, 78.40.−q, 78.68.+m

I. INTRODUCTION

Optical properties of metallic nanostructures have attracted considerable attention.[1–3] Colloidal gold spheres in liquid represent one of the simplest metallic nanostructures. They exhibit a ruby-red color because the cooperative oscillation of free electrons in the nanostructure is resonant with green light.[4] This resonance phenomenon is termed localized surface plasmon resonance (LPR). Under the LPR condition, a large electric field is generated around nanospheres. When two gold nanospheres are aggregated to form a dimer with a gap distance of a few nanometers, their electromagnetic interaction results in the appearance of another redshifted LPR band.[5,6] Theoretical calculations predict that a strong electric field enhanced 100 times is generated in the nanogap of a silver dimer. This large electric field is used for single-molecule Raman spectroscopy.[7–9]

The optical properties of surface-immobilized gold nanospheres (SIGNs) above a metallic surface with a gap distance of a few nanometers are similar to those of dimer gold nanospheres because the nanospheres are mirrored in the metallic surface. The redshifted band can be observed in reflection absorption (RA) spectra. The theoretical calculations also reveal that the electric field in the nanogap is significantly intensified similar to a dimer. These systems have been theoretically investigated by several groups[10–12] and experimentally studied by other groups employing linear optical spectroscopy.[13,14] Okamoto *et al.* formed SIGNs above a gold surface by using a self-assembled monolayer (SAM) of aminoethanethiol as a spacer; they also demonstrated that the amount of redshift depends on the size of gold nanospheres.[14] These experimental results imply that the optical properties of the SIGN systems are similar to those of nanosphere dimers due to the electromagnetic interaction between the nanospheres and their images in a metallic surface. Therefore, SIGNs above a metal might serve as a promising system to investigate the optical properties of metallic nanostructures.

Experimental measurements of enhanced electric fields in nanostructures are essential to gain a detailed understanding of the electromagnetic interaction. Although some studies based on fluorescence spectroscopy[15,16] and metallic-tip-enhanced light scattering measurements[17–19] have been conducted, they did not produce quantitative values of enhancement factors since fluorescence occasionally quenches at a metallic surface and these are incoherent physical processes. Nonlinear optical effects are coherent and devoid of quenching even when a radiation source is located near a metallic surface. Therefore, they represent a powerful tool to investigate the electric field in nanostructures. In this paper, we performed both RA spectroscopy and optical second-harmonic generation (SHG) measurements for SIGNs above metallic surfaces. The experimental results are discussed using theoretical calculations obtained by considering multipolar interactions based on a quasistatic approximation. SHG is a type of second-order nonlinear optical effect; it is prohibited in a system with an inversion center under the electric dipole approximation.[20] Metallic surfaces exhibit SHG activity that primarily originates from the noncentrosymmetry of a surface and an interface.[21–23] Hence, the SHG activity in isolated gold nanospheres and their dimers is small due to the presence of an inversion center although SHG from quardrupoles should be taken into account in a detailed consideration.[24,25] Actually our preliminary experiments have revealed that SIGNs above a dielectric substrate of silica show a small SHG response. The SHG activity in SIGN systems above a metal might be absent due to their similarity with gold nanosphere dimers. However, SIGN systems exhibit considerably higher SHG activity than metallic surfaces, as demonstrated in this paper. Further, we performed theoretical

calculations of the RA spectra and SHG, which are essential to understand the enhancement in SHG in detail.

II. EXPERIMENT

A SIGN system comprises gold nanospheres immobilized above a metallic surface supported by aminoalkanethiol SAMs $[H_2N(CH_2)_nSH]$ with different chain lengths ($n=2,6,8,11$). Two types of substrates—gold and silver—are used to investigate the optical properties of the SIGN systems above a metallic substrate with different dielectric constants. SIGNs above gold obtained using a SAM of $H_2N(CH_2)_nSH$ are termed SIGN-(n)-gold and SIGNs above silver are termed SIGN-(n)-silver, where n is the number of CH_2 groups in the aminoalkanethiol. The number n is suppressed unless necessary.

The gold nanospheres were prepared by the reduction of $NaAuCl_4$.[26] An aqueous solution of 0.254 mM $NaAuCl_4$ (100 ml) was maintained at 95 °C in a water bath, and an aqueous solution of 33.3 mM citrate (5.0 ml) was added with stirring. The color of the solution immediately changed to ruby red. It was further stirred for 10 min, and cooled to room temperature. The diameter of the resulting gold nanospheres was 40.8±12.6 nm. Aminoethanethiol $[H_2N(CH_2)_2SH$, AET], aminohexanethiol $[H_2N(CH_2)_6SH$, AHT], aminooctanethiol $[H_2N(CH_2)_8SH$, AOT], and aminoundecanethiol $[H_2N(CH_2)_{11}SH$, AUT] were used for surface modification. They were dissolved in ethanol and used as a 1 mM solution.

Gold and silver substrates were prepared by depositing a 300-nm-thick gold or silver film on a silica substrate by a vacuum evaporation method under a base pressure lower than 10^{-3} Pa. In order to deposit aminoalkanethiol SAMs, the substrate was immersed in the aminoalkanethiol solution for 2 h, followed by rinsing with ethanol to remove excess aminoalkanethiol molecules. Gold nanospheres were deposited on the substrate by immersing it in their solution for 2 h. The area occupied by the gold nanospheres was evaluated by scanning electron microscopy (SEM).

The RA spectra were obtained with an MCPD-3000 spectrometer (Otsuka Electronics Co., Ltd., Japan). Light from a halogen lamp (150 W) was guided to the surface by an optical fiber and was passed through a polarizer. Reflected light was conveyed to the spectrometer by another optical fiber. Reflected spectra at the bare metallic surface without any gold nanospheres were used as a reference.

The SHG measurements were carried out with the optical setup shown in Fig. 1(a). A neodymium-doped yttrium aluminum garnet (Nd:YAG) laser (LS-2135, LOTIS TII, Ltd.) was used as the light source; it was operated at its fundamental wavelength ($\lambda=1064$ nm) and at a frequency of 10 Hz with a pulse width of 10 ns. The polarization of the incident light was chosen with a combination of a half-wave plate and Glan laser prism. The angle of incidence was fixed at 45°. The laser light was incident on the sample surface with no focusing; the spot size at the sample surface was 5 mm in diameter. The power density of the fundamental light was reduced to be approximately 27 mJ/cm^2 with neutral density filters. We checked that the samples were not damaged with this power density. The reflected SH light was detected using an R-955 photomultiplier tube (PMT, Hamamatsu Photonics K.K., Japan) after the removal of fundamental light with color and interference filters. The polarization of the reflected light was selected using a linear polarizer. The PMT output was averaged by a boxcar integrator for 10 s.

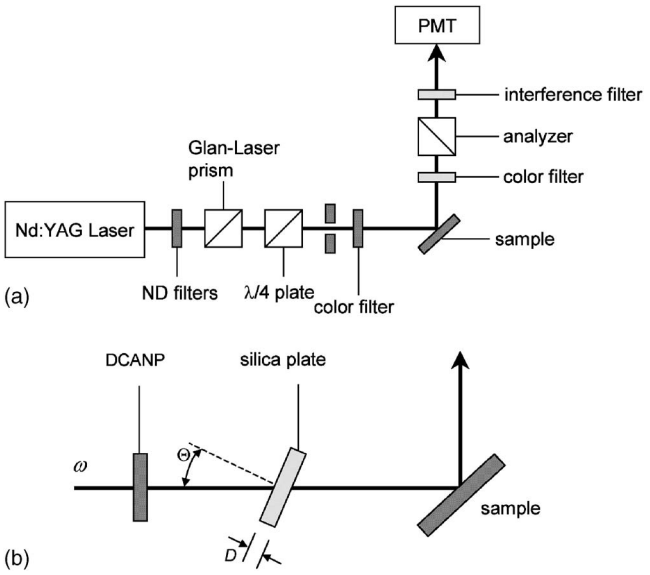

FIG. 1. (a) Optical setup for SHG measurements. (b) Optical geometry for phase measurements of SHG.

SHG phase measurements were performed by measuring interference profiles of SHG light using a local oscillator, as shown in Fig. 1(b).[27–29] A docosylaminonitropyridine Langmuir-Blodgett (DCANP LB) film comprising 10 monolayers[30] was used as the local oscillator; it is a useful SHG source for phase measurements.[31] The largest second-order susceptibility component of the DCANP LB film is along the dipping direction of the LB film. A silica plate with a thickness of approximately 1 mm was installed between the local oscillator and the sample in order to vary the retardation of the SH light relative to the fundamental light. This is because the refractive index of the silica plate for fundamental light, n^{ω}, slightly differs from that for the SHG light, $n^{2\omega}$. The retardation is varied by rotating the silica plate in order to obtain an SHG interference profile relative to the angle of incidence of the silica plate.[31]

III. THEORY

A. Local electric field

We consider the local field associated with the LPR in SIGNs above a metal. Suppose that a single gold nanosphere with a radius R is located above a substrate with a gap distance d. The cross section of this system normal to the substrate is illustrated in Fig. 2(a). Mediums 1, 2, and 3 refer to the ambience, substrate, and nanosphere, respectively. The dielectric constant of medium i is denoted by ε_i. Based on the description by Wind *et al.*,[12] spherical coordinates (ρ, θ, ϕ) are used to describe the local electric field at a point P in

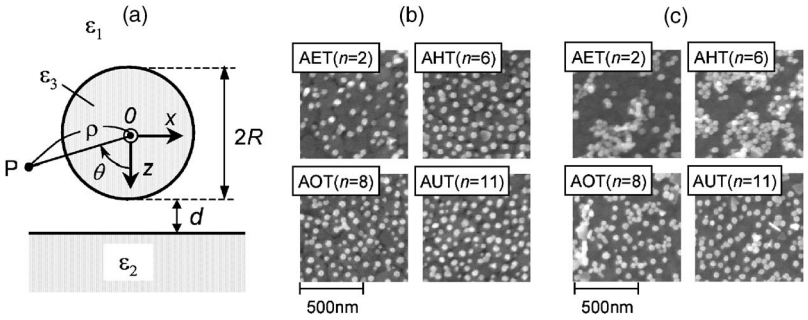

FIG. 2. (a) Geometry for theoretical calculations of SIGNs above a metallic surface. SEM images of (b) SIGN-(n)-gold and (c) SIGN-(n)-silver (n=2,6,8,11).

medium 1. In order to generalize the description, a reduced potential at the point P, ψ, in medium 1 is introduced as

$$\psi = -\frac{V}{E_0 R}, \tag{1}$$

where V is the potential and E_0 is the external electric field. The reduced potential induced by the electric field perpendicular to the surface, $\psi_\perp$, can be written as a series of multipoles as follows:[12]

$$\psi_\perp = r\cos\theta + \sum_{j=0}^{\infty}\left(\frac{A_j P_j^0(\cos\theta)}{r^{(j+1)}} + A_j' V_j^0(r,\cos\theta)\right). \tag{2}$$

The reduced potential induced by an in-plane electric field, $\psi_\parallel$, is expressed as follows:

$$\psi_\parallel = r\sin\theta\cos\phi + \sum_{j=0}^{\infty}\left(\frac{B_j P_j^1(\cos\theta)\cos\phi}{r^{(j+1)}} + B_j' V_j^1(r,\cos\theta)\cos\phi\right), \tag{3}$$

where A_j, B_j, A_j', and B_j' are the multipole coefficients and r is the distance from the origin normalized by the radius of the nanosphere $R(r=\rho/R)$. $P_j^m(\cos\theta)$ is the associated Legendre function of the first kind with a degree j and order m. $V_j^m(r,\cos\theta)$ is defined by the following equation:

$$V_j^m(r,\cos\theta) = \frac{P_j^m\left(\frac{r\cos\theta - 2r_0}{(r^2 - 4rr_0\cos\theta + 4r_0^2)^{1/2}}\right)}{(r^2 - 4rr_0\cos\theta + 4r_0^2)^{(j+1)/2}} \quad (m=0,1), \tag{4}$$

where $r_0=d/R$. The multipole coefficients A_j and B_j are determined from the following linear equations:

$$\sum_{j=1}^{\infty}\left(\delta_{kj} + \frac{k(k+j)!(\varepsilon_2-\varepsilon_1)(\varepsilon_1-\varepsilon_3)}{k!j!(2r_0)^{k+j+1}(\varepsilon_2+\varepsilon_1)((k+1)\varepsilon_1+k\varepsilon_3)}A_j\right) = \frac{\varepsilon_1-\varepsilon_3}{2\varepsilon_1+\varepsilon_3}\delta_{k1}, \tag{5a}$$

$$\sum_{j=1}^{\infty}\left(\delta_{kj} + \frac{k(k+j)!(\varepsilon_2-\varepsilon_1)(\varepsilon_1-\varepsilon_3)}{(k+1)!(j-1)!(2r_0)^{k+j+1}(\varepsilon_2+\varepsilon_1)((k+1)\varepsilon_1+k\varepsilon_3)}B_j\right) = \frac{\varepsilon_1-\varepsilon_3}{2\varepsilon_1+\varepsilon_3}\delta_{k1}. \tag{5b}$$

A_j' and B_j' are obtained from A_j and B_j as follows:

$$A_j' = \frac{\varepsilon_1-\varepsilon_2}{\varepsilon_1+\varepsilon_2}(-1)^j A_j, \tag{6a}$$

$$B_j' = \frac{\varepsilon_1-\varepsilon_2}{\varepsilon_1+\varepsilon_2}(-1)^{j+1} B_j. \tag{6b}$$

It is convenient to use Cartesian coordinates to decide the local electric fields at the surface of the substrate. A local electric field $\mathbf{e}$ at a point S (r,θ,ϕ) at the substrate surface can be written in Cartesian coordinates as follows:

$$e_x = \sin\theta\cos\phi\frac{\partial\psi}{\partial r} + \frac{\cos\theta\cos\phi}{r}\frac{\partial\psi}{\partial\theta} - \frac{\sin\phi}{r\sin\theta}\frac{\partial\psi}{\partial\phi}, \tag{7a}$$

$$e_y = \sin\theta\sin\phi\frac{\partial\psi}{\partial r} + \frac{\cos\theta\sin\phi}{r}\frac{\partial\psi}{\partial\theta} + \frac{\cos\phi}{r\sin\theta}\frac{\partial\psi}{\partial\phi}, \tag{7b}$$

$$e_z = \cos\theta\frac{\partial\psi}{\partial r} - \frac{\sin\theta}{r}\frac{\partial\psi}{\partial\theta}. \tag{7c}$$

On the other hand, it is convenient to use spherical coordinates to describe the local electric fields at the surface of the nanosphere. Therefore, the reduced electric field $\mathbf{e}$ can be expressed as follows:

$$\mathbf{e} = (e_r, e_\theta, e_\phi) = \left(\frac{\partial\psi}{\partial r}, \frac{1}{r}\frac{\partial\psi}{\partial\theta}, \frac{1}{r\sin\theta}\frac{\partial\psi}{\partial\phi}\right). \tag{8}$$

B. Absorption spectra of the SIGN system

The absorption efficiency C_{abs} was calculated based on the procedure of Okamoto *et al.*[14] The polarizability of the SIGN above a metal for p-polarized incident light is given by

$$\alpha_\perp = 4\pi\varepsilon_1 R^3 A_1, \tag{9a}$$

$$\alpha_{\parallel} = 4\pi\varepsilon_1 R^3{}_1 B_1, \tag{9b}$$

where A_1 and B_1 are given by Eq. (5) and $\alpha_{\perp}$ and $\alpha_{\parallel}$ are the polarizabilities in the z and x directions, respectively. Further, C_{abs} is the sum of the contributions of both the perpendicular and parallel components for an arbitrary polarization. By considering the reflection of the incident light at the substrate surface, we determined the absorption efficiency for p-polarized incident light as follows:

$$C_{\mathrm{abs}} = \frac{2}{\lambda_0 R^2}\{[\mathrm{Im}(|1+F_p|\sin\theta\alpha_{\perp})]^2 + [\mathrm{Im}(|1-F_p|\cos\theta\alpha_{\parallel})]^2\}, \tag{10}$$

where θ is the angle of incidence, and F_p is the Fresnel coefficient of reflection for p-polarized light at the surface.

C. SHG from SIGN systems

The SHG field $E^{2\omega}$ generated from a single SIGN system by the fundamental field E^{ω} can be written in the following manner:

$$E^{2\omega} = \int_s L_2^{2\omega}\chi_2 : (L_2^{\omega}E^{\omega})(L_2^{\omega}E^{\omega})d\sigma + \int_p L_3^{2\omega}\chi_3 : (L_3^{\omega}E^{\omega})(L_3^{\omega}E^{\omega})d\sigma, \tag{11}$$

where χ_2 and χ_3 denote the surface susceptibilities of the metallic substrate and gold nanospheres, respectively, and $d\sigma = r\sin\theta\, d\theta\, d\phi$. The first and second terms represent integrals over the surface areas of the metallic substrate and gold nanosphere, respectively. L_2^{Ω} and L_3^{Ω} denote local field factors at a frequency Ω ($\Omega=\omega,2\omega$) obtained from the calculated local electric fields. The local field factors at ω are used to determine the local field with an electric field of incident light E^{ω}. They depend on position and frequency. The local field factors at 2ω are obtained similarly.

D. Phase measurement of SHG light

The phase measurements are performed using SHG interferometry. As shown in Fig. 1(b), the SHG measurements are performed by varying the optical path between the two SHG sources and rotating a silica plate with refractive index $n_{\mathrm{silica}}^{\Omega}$ at a frequency Ω. The total SHG intensity $I^{2\omega}$ detected in the phase measurement is written as follows:

$$I^{2\omega} = |E_{\mathrm{LO}}^{2\omega}|^2 + |E_{\mathrm{sample}}^{2\omega}|^2 + 2|E_{\mathrm{LO}}^{2\omega}||E_{\mathrm{sample}}^{2\omega}|\cos\Delta(\Theta_1^{\omega}). \tag{12}$$

Here, $E_{\mathrm{LO}}^{2\omega}$ and $E_{\mathrm{sample}}^{2\omega}$ denote the SHG fields from the local oscillator and sample, respectively. The retardation of the SH light relative to the fundamental light, $\Delta(\Theta_1^{\omega})$, is expressed as a function of the incident angle to the silica plate Θ_1^{ω}:[28,31,32]

$$\Delta(\Theta_1^{\omega}) = \frac{2\pi D}{\lambda_0^{2\omega}}\left(\frac{1}{\cos\Theta_2^{2\omega}}[n_{\mathrm{silica}}^{2\omega} - \cos(\Theta_1^{2\omega}-\Theta_2^{2\omega})] - \frac{1}{\cos\Theta_2^{\omega}}[n_{\mathrm{silica}}^{\omega} - \cos(\Theta_1^{\omega}-\Theta_2^{\omega})]\right) + \Delta_0, \tag{13}$$

where Θ_2^{Ω} is the angle of refraction at a frequency Ω ($\Omega=\omega,2\omega$) in the silica plate; D is the thickness of the silica plate; $\lambda_0^{2\omega}$ is the vacuum wavelength of SHG light; and Δ_0 is a constant term independent of Θ_1^{ω}. The negligible dispersion in air yields the relation $\Theta_1^{\omega}\approx\Theta_1^{2\omega}$. The difference between Θ_2^{ω} and $\Theta_2^{2\omega}$ due to the frequency dispersion of silica results not only in the difference in retardation within the silica substrate but also in retardation in air. Therefore, $\Delta(\Theta_1^{\omega})$ increases with an increase in the incident angle of the silica plate, Θ_1^{ω}.

IV. RESULTS AND DISCUSSION

A. Reflection absorption spectroscopy

Figure 2 shows the SEM images of SIGN-(n)-gold samples ($n=2,6,8,11$). The gold nanospheres appear to be dispersed uniformly with the following surface coverages: $\sigma_2=0.11$, $\sigma_6=0.15$, $\sigma_8=0.17$, and $\sigma_{11}=0.20$, where the subscript refers to the number of CH_2 units in aminoalkanethiol. The low coverage of SIGN-(2)-gold observed in the SEM image suggests a poor-quality sample. Furthermore, Fig. 2(c) shows the SEM images of SIGN-(n)-silver. The nanospheres appear to be uniformly dispersed in SIGN-(8)-silver and SIGN-(11)-silver, although they are partially aggregated in SIGN-(6)-silver and are highly aggregated in SIGN-(2)-silver. The surface coverages of $\sigma_8=0.17$ and $\sigma_{11}=0.16$ are evaluated from the SEM images. It should be noted that the quality of the samples of SIGN-(2)-silver and SIGN-(6)-silver is not sufficient for the SHG measurements.

Figure 3(a) shows the p-polarized RA spectra of SIGN-(n)-gold in air at an incident angle of 45°. Two absorption bands are observed in each spectrum: one at approximately 520 nm (the first band) and the other at 600–700 nm (the second band). In the first band, two contributions are found to overlap. One is attributed to the resonance of the multipolar interaction between the nanosphere and the substrate surface, which has a normal component to the surface. The other is similar to the resonance of isolated nanospheres with both in-plane and normal components. Therefore, the first band can generally be observed with both p- and s-polarized light. The second band is redshifted from the first one and is attributed to the resonance due to the multipolar interaction. The observation of the second band only in p-polarized excitation indicates that it has a normal component. The peak wavelength strongly depends on the thickness of the SAMs used as a spacer.

The RA spectra are simulated using Eq. (10), as shown in Fig. 4(a). The absorption efficiency in air is calculated for four reduced gap distances d/R ranging from 1/40 to 1/10. The ambient dielectric constant $\varepsilon_1=1.3$ was used as the most appropriate average value of air and the SAMs were used as

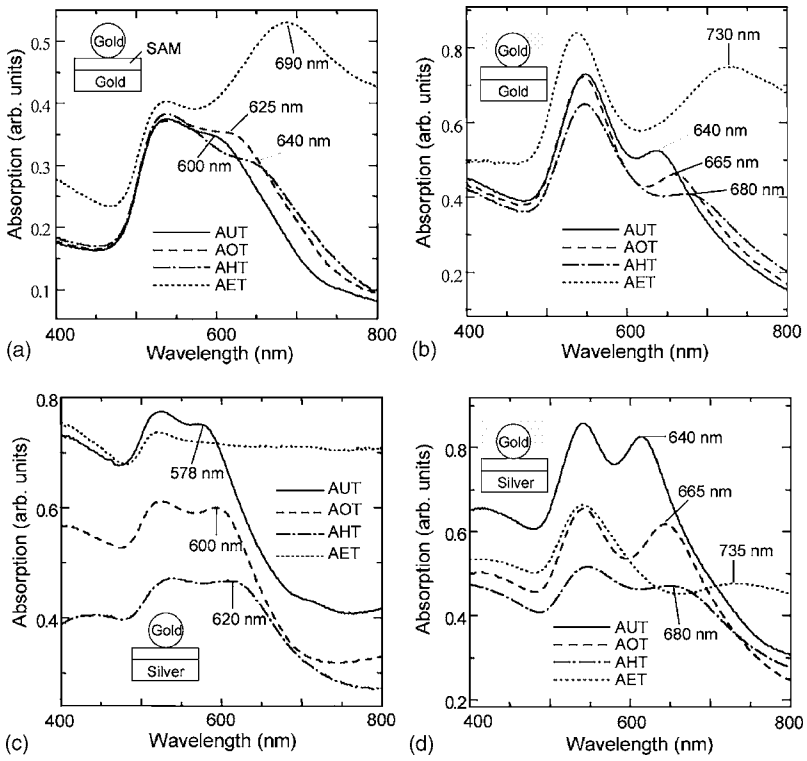

FIG. 3. RA spectra of various SIGN systems at an incident angle of 45°. (a) SIGN-(n)-gold in air, (b) SIGN-(n)-gold in water, (c) SIGN-(n)-silver in air, and (d) SIGN-(n)-silver in water.

a spacer in accordance with a suggestion in a previous paper.[14] The amount of redshift increases with a decrease in the gap distance. The gap distance produced by the AET (n =2) SAM is 0.8 nm according to the molecular model with the assumption that the molecular long axis is aligned normal to the surface. The corresponding peak wavelength is calculated to be 680 nm, which is in good agreement with the experimental results shown in Fig. 3(a). The gap distances produced by AHT (n=6), AOT (n=8), and AUT (n=11) SAMs are 1.3, 1.6, and 2.0 nm, respectively. The corresponding peak wavelengths are calculated to be 640, 620, and 600 nm, respectively; these values are also in good agreement with the experimental results shown in Fig. 3(a). On the other hand, the intensity and shape of the peak in the actual spectra are not in good agreement, because of the distribution of the nanosphere size.

Figure 3(b) shows the RA spectra of SIGN-(n)-gold in water. Since the surrounding dielectric constant of water is

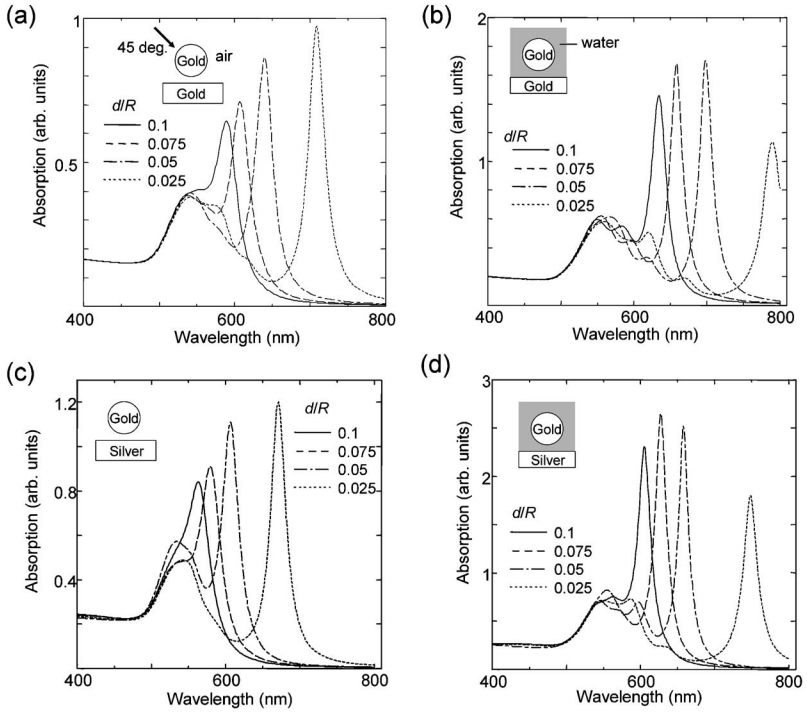

FIG. 4. Calculated RA spectra at an incident angle of 45°. (a) SIGN-(n)-gold in air, (b) SIGN-(n)-gold in water, (c) SIGN-(n)-silver in air, and (d) SIGN-(n)-silver in water.

larger than unity, the second band appears at a wavelength that is approximately 40 nm greater than that in air. As shown in Fig. 4(b), the redshift of the second peak is also simulated; this shift is slightly larger than that in the experimental results. A possible reason for this discrepancy is that the nanosphere is not completely covered with water because gaps are produced between the nanosphere and the SAM; therefore, the average dielectric constant is slightly smaller than that of water. This possibility is consistent with our experimental results of SHG that the SIGNs are not completely covered with chromophoric SAMs when the substrate is simply immersed in a solution.[33] Another possible reason is a slight expansion of the nanogap in water. The hydrophilic surface of the nanosphere yields good wetability for water.

Similarly, SIGN-(n)-silver with various n values is examined in air and water, as shown in Figs. 3(c) and 3(d), respectively. The corresponding spectra calculated in the same manner are shown in Figs. 4(c) and 4(d). In Fig. 3(c), the second absorption band of SIGN-(2)-silver in air is absent because of the aggregation of the nanospheres, as shown in the SEM image. However, a broad peak of SIGN-(2)-silver in water is observed at 735 nm. The amount of redshift of the second band of SIGN-(n)-silver is smaller than that in the corresponding spectra of SIGN-(n)-gold in air and water. The imaginary part of the dielectric constant of silver is very small and therefore, it behaves as an ideal metal even in the visible light region. The images of the nanospheres on the silver surface are perfect in comparison with those in the gold surface. The lines of electric force from the gold nanospheres are normal to the surface. On the other hand, a relatively large imaginary part of the dielectric constant of gold causes an imperfect image in the gold surface; namely, the lines of electric force from the gold nanosphere are oblique to the gold surface. Hence, the effective gap distance between the SIGN and its image may be reduced, thereby resulting in a larger redshift than that of a silver surface.

B. SHG measurements

Figure 5(a) shows the SHG intensity from SIGN-(n)-gold normalized by that from a bare gold surface covered with aminoalkanethiol SAMs without any SIGNs. Further, Fig. 5(b) shows the SHG intensity from SIGN-(n)-silver normalized by that from a bare silver surface. The normalized SHG intensity from SIGN-(n)-gold samples ($n=6,8,11$) is 6–7, although the coverage of the gold nanospheres, σ, is significantly smaller than unity. The SHG intensity from SIGNs-(n)-silver samples ($n=8,11$) is nearly the same as that from a bare gold surface. Partially aggregated nanospheres observed in the SEM images do not contribute to the SHG response. The relatively large SHG intensity from SIGN-(2)-silver in air may be due to hot spots in the aggregate nanospheres.

The observed SHG intensity $I^{2\omega}$ from the SIGN samples can be written as follows:

$$I^{2\omega} = |\sigma E^{2\omega}_{\mathrm{SIGN}} + (1-\sigma)E^{2\omega}_{\mathrm{bare}}|^2, \tag{14}$$

where $E^{2\omega}_{\mathrm{SIGN}}$ is the SHG field from a unit area of the SIGN surface and $E^{2\omega}_{\mathrm{bare}}$ is that from the metallic surface with no

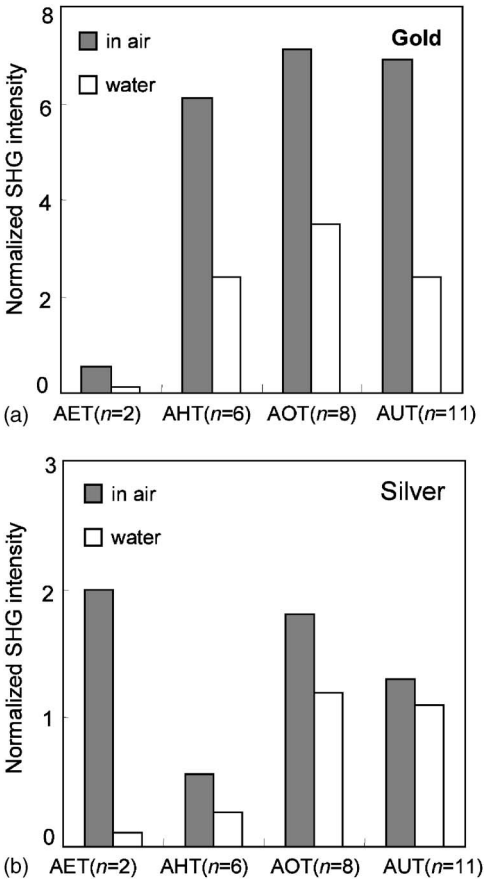

FIG. 5. Experimental results of SHG intensity measured in air and water for (a) SIGN-(n)-gold and (b) SIGN-(n)-silver.

SIGNs. We introduce a field enhancement factor due to the presence of the gold nanospheres, $A^{2\omega}$; it is defined by

$$A^{2\omega} = \frac{E^{2\omega}_{\mathrm{SIGN}}}{E^{2\omega}_{\mathrm{bare}}} = \frac{|E^{2\omega}_{\mathrm{SIGN}}|}{|E^{2\omega}_{\mathrm{bare}}|}e^{i\delta}. \tag{15}$$

Since the phase of $E^{2\omega}_{\mathrm{SIGN}}$ is not necessarily the same as that of $E^{2\omega}_{\mathrm{bare}}$, the relative phase difference between them, δ, should be considered. The phase measurements of SHG in air were performed using the optical geometry shown in Fig. 1(b) for SIGN-(n)-gold. It was determined that E_{SIGN} and E_{bare} are almost in phase. Therefore, we neglect the phase difference in the evaluation of $A^{2\omega}$ values.

Using the σ values obtained from the SEM images, we determined the absolute values of $A^{2\omega}$ and they are summarized in Table I. In SIGN-(n)-gold ($n=8,11$), the enhancement factors $|A^{2\omega}|$ in air are greater than 10, whereas those in water are smaller. The $A^{2\omega}$ values of SIGN-(2)-gold are negative. The negative enhancement factor means that the SHG intensity from the SIGN system is smaller than that from a bare gold surface. There are two possible reasons: one is that the SHG fields of the SIGNs and bare gold surface are out of phase. The theoretical calculation described below does not predict such a large phase change with the parameters of SIGN-(2)-gold. Hence this is not the main reason for the negative value. Another possible reason is that the SIGN-(2)-gold sample of bad quality weakens the SHG intensity.

TABLE I. Absolute value of the field enhancement factor $|A^{2\omega}|$ for SIGN-(n)-gold in air and water. It should be noted that the $A^{2\omega}$ values of SIGN-(2)-gold are negative, since the SHG intensity is smaller then that of the bare gold surface, as shown in Fig. 5.

SIGN-(2)-gold	SIGN-(6)-gold	SIGN-(8)-gold	SIGN-(11)-gold
	In air		
−1.30	10.5	11.0	9.33
	In water		
−4.92	4.66	6.28	3.87

The RA spectrum of SIGN-(2)-gold in Figs. 3(a) and 3(b) has a large offset at 600–800 nm, probably due to aggregation of the gold nanospheres. The aggregated parts do not contribute to the SHG response, resulting in a decrease in the SHG intensity. The values of $|A^{2\omega}|$ for the SIGN-(n)-silver are summarized in Table II. The values of $|A^{2\omega}|$ for SIGN-(2)-silver and SIGN-(6)-silver cannot be obtained because the σ values cannot be determined from the SEM images of the poor-quality samples. In SIGN-(6)-silver and SIGN-(8)-silver, the particles are highly dispersed; however, the $|A^{2\omega}|$ values are smaller than those of SIGN-(n)-gold due to the partial aggregation of silver nanospheres.

TABLE II. Absolute value of field enhancement factor $|A^{2\omega}|$ for the SIGN-(n)-silver system in air and in water. Note that the data for the SIGN-(2)-silver and SIGN-(6)-silver samples are not available since the surface coverage σ of the nanospheres cannot be estimated due to aggregation of the nanospheres, as shown in the SEM images.

SIGN-(8)-silver sample	SIGN-(11)-silver sample
In air	
2.89	1.47
In water	
1.79	1.34

C. Calculation of local field

We discuss the results for the calculated local electric fields. In the SIGN systems, it is calculated that the electric field induced by a surface-normal electric field is much larger than that by the in-plane component. The actual ratio of the electric field is 3700:1 at the nanogap. Hence we regard the coefficients B in Eq. (5) as negligibly small, and we evaluate only the coefficients A in this study. The dielectric constants used in the calculations are provided in the literature.[34] Figure 6(a) shows the absolute value and phase of the electric field in the r direction at the surface of the

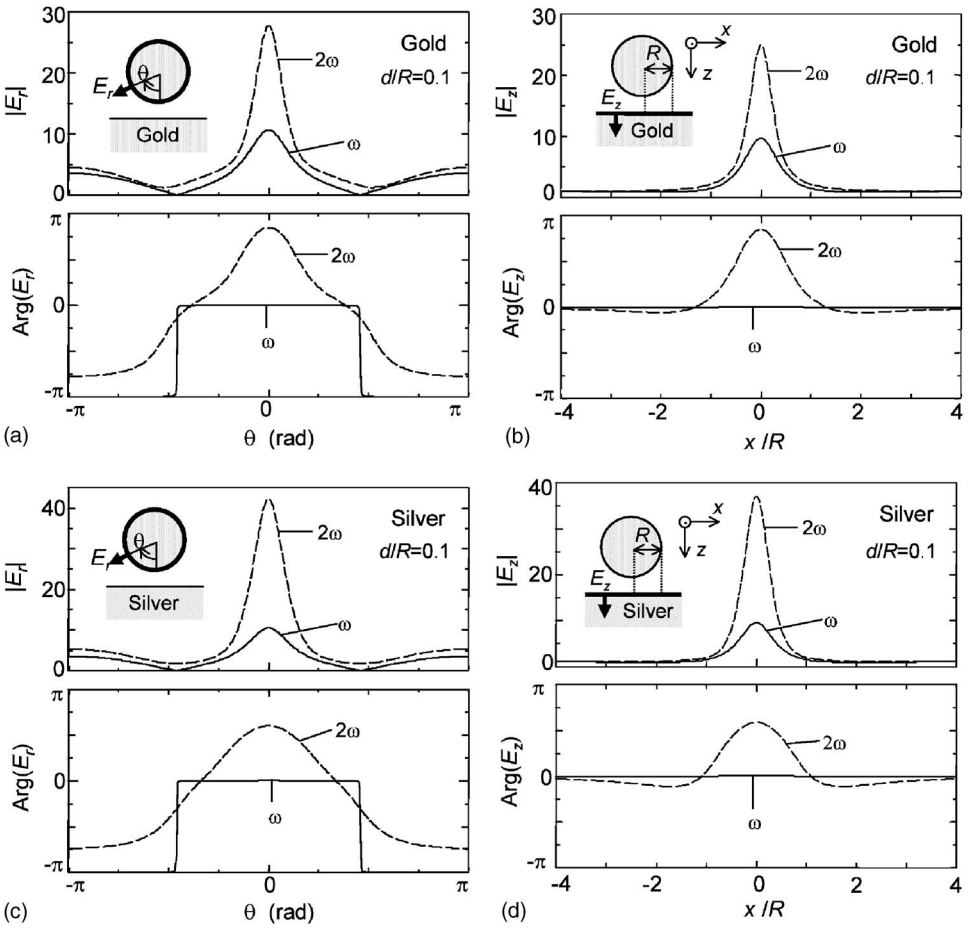

FIG. 6. Calculated electric field and phase in the SIGN systems at $d/R=1/10$. The calculated results at ω are plotted with a solid line and those at 2ω with a dashed line. (a) Absolute value and phase of the enhanced electric field in the r direction at the surface of the nanosphere in the SIGN-gold system plotted as a function of θ, (b) the z direction at the gold surface of the substrate in the SIGN-gold system plotted as a function of x/R, (c) the r direction at the surface of the nanosphere in the SIGN-silver system plotted as a function of θ, and (d) the z direction at the silver surface of the substrate in the SIGN-silver system plotted as a function of x/R.

gold nanosphere at $d/R=1/10$ as a function of θ. $|E_r|$ exhibits two peaks: one at $\theta=0$ and the other at $\theta=\pi$. The field at $\theta=0$ is enhanced by a factor of 10 at ω and 28 at 2ω. The field is minimum near $\theta=\pi/2$ and $-\pi/2$; however, it deviates slightly from $\theta=\pi/2$ and $-\pi/2$ due to the surface effect. The full width at half maximum (FWHM) in θ is approximately $\pi/4$ for ω and $\pi/6$ for 2ω. The profiles of $|E_r|$ at ω and 2ω are identical with the exception that the absolute field at 2ω is larger. However, the phase profile at ω is different from that at 2ω. The phase at ω is constant at 0 or at $-\pi$; this implies that E_r is real. The discontinuous jumps at approximately $\theta=-(1/2)\pi$ and $\theta=(1/2)\pi$ occur due to the use of spherical coordinates. In contrast, the phase at 2ω continuously varies from $-(3/4)\pi$ to $(3/4)\pi$ in the region of $\theta=-(1/2)\pi$ to $\theta=(1/2)\pi$. This large phase change is composed of two components. By eliminating a phase change of π occurring due to spherical coordinates, a large phase change with a peak at $\theta=0$ originating from the multipolar LPR is observed. The constant phase of the other region corresponding to the upper hemisphere surface involves the resonance character of isolated nanospheres, which enhances the electric field without any phase change.

Figure 6(b) shows the $|E_z|$ and $\arg(E_z)$ profiles of the gold substrate surface. It should be noted that the direction of E_z is the same as that of E_r at ω and $\theta=0$. Each $|E_z|$ profile at ω and 2ω exhibits a peak at $x/R=0$ with a FWHM of 0.4. The maximum values of $|E_z|$ are 10 at ω and 25 at 2ω. Similar to the E_r profiles, the phase profile of E_z at 2ω varies significantly and the profile at ω is constant at zero. Both enhancement of the electric field and the large phase change is observed under the resonance condition at 2ω, whereas only enhancement of the electric field is observed at ω. The phase response is more sensitive to the resonance condition.

In addition, the values of $|E_z|$ and $\arg(E_z)$ for the SIGN-silver system at $d/R=1/10$ are calculated and plotted in Figs. 6(c) and 6(d). The profiles are similar to those of the SIGN-gold system with the exception of the following. The maximum $|E_r|$ and $|E_z|$ values are larger than those of gold, while the phase change is smaller. The electric field is enhanced considerably by stronger resonance due to the small imaginary part of the dielectric constant of silver. This part is also responsible for the small phase change in the SIGN-silver system in comparison with that in the SIGN-gold system.

D. Calculation of SHG response

The absolute value of the enhancement factor $|A^{2\omega}|$ of the SIGN systems is calculated using Eq. (11). The first term of this equation is integrated within the cross-sectional circular area of the metallic surface with a radius R below the nanosphere since most of the enhanced field is limited within this area, as shown in Fig. 6(b). Two mechanisms can be considered to account for the enhancement in the SHG intensity. One is that the presence of SIGNs above a metallic substrate increases the surface susceptibility, and the other is that the local electric field in the SIGN system increases due to LPR. The present calculation is based on the second mechanism because it is difficult to consider the former mechanism. The

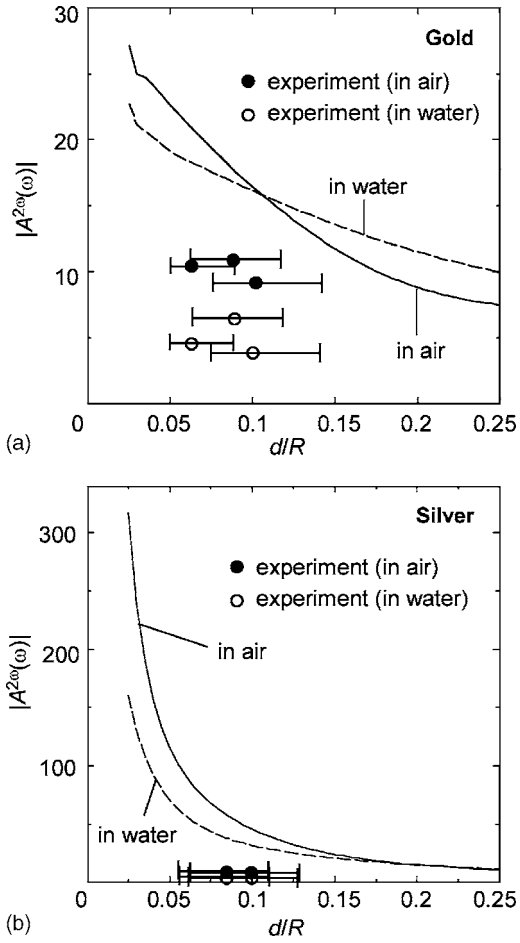

FIG. 7. Calculated field enhancement factor $|A^{2\omega}|$ in air (solid line) and water (dashed line) plotted as a function of d/R for (a) SIGN-gold and (b) SIGN-silver systems. The experimental results listed in Tables I and II are also plotted. The error bars indicate the standard deviation of the nanosphere size.

calculations of SHG for SIGN-gold were performed under the assumption that $|\chi_2|=|\chi_3|$ since the nanospheres and substrate are composed of the same material. Figure 7(a) shows the $|A^{2\omega}|$ values of the SIGN-gold as a function of the gap distance in air and water. The $|A^{2\omega}|$ value is 10–20, it increases with a decrease in the gap distance, and its value in air is almost the same as that in water. The experimental results listed in Table I are also plotted in the figure. The error bar indicates the standard deviations of the nanosphere size. Both theoretical and experimental results are in rough agreement and are within the same order. A possible reason for the disagreement is that the macroscopic local field is smaller than the external field. Since the polarizability of the SIGN system is larger than unity, the effective field in the z direction is smaller than the external field, due to continuity of normal component of the displacement fields.[35] One may also find that the theoretical results do not reproduce the experimental in the case of the SIGN systems in water. This tendency is also observed in the RA spectra. The possible reason is that the nanogap slightly expanded in water probably since the surface of the nanospheres is hydrophilic and high wetability to water.

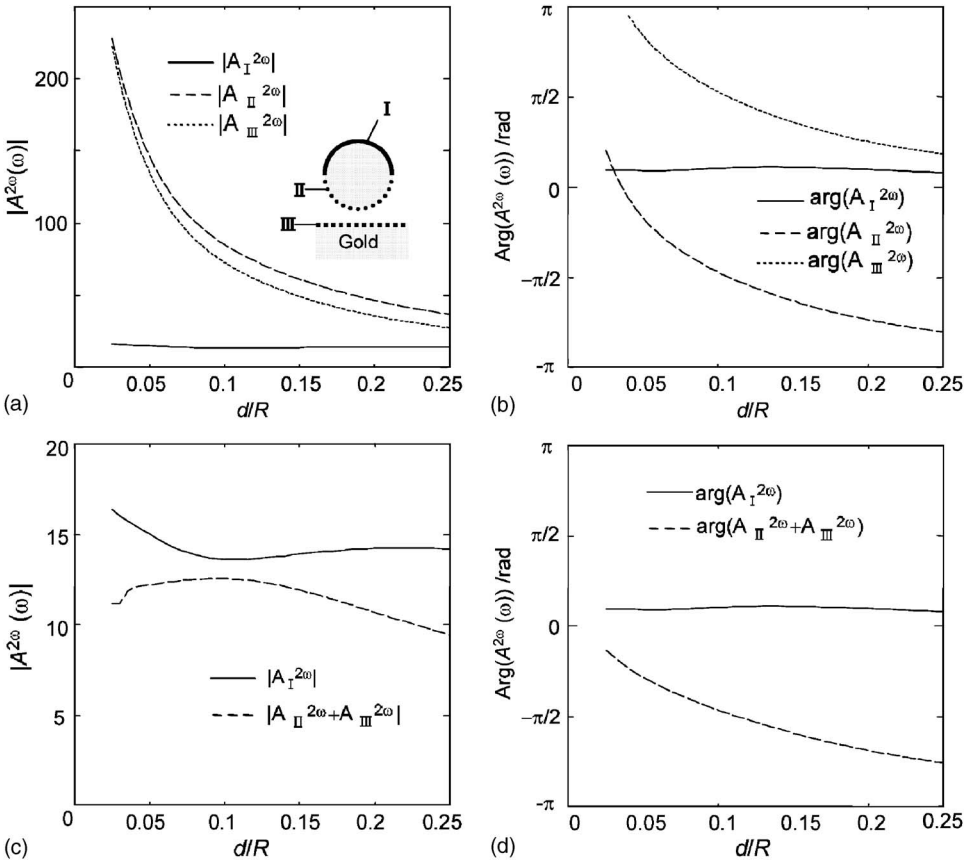

FIG. 8. Result of detailed calculation of $|A^{2\omega}|$ for SIGN-gold in air plotted as a function of d/R. The SIGN system is divided into three parts; the surface of the upper hemisphere of the nanosphere (part I, $A_{\mathrm{I}}^{2\omega}$), the surface of the lower hemisphere (part II, $A_{\mathrm{II}}^{2\omega}$), and the surface of the substrate (part III, $A_{\mathrm{III}}^{2\omega}$), as shown in the inset of (a). (a) Absolute value of the enhancement factor for each part. (b) Phase of the enhancement factor for each part. (c) Comparison between the field enhancement factor for part I $|A_{\mathrm{I}}^{2\omega}|$ (solid line) and that in the nanogap region $|A_{\mathrm{II}}^{2\omega}+A_{\mathrm{III}}^{2\omega}|$ (dashed line). (d) Calculated phases for part I plotted with a solid line and those in the nanogap region plotted with a dashed line.

Figure 7(b) shows the $|A^{2\omega}|$ values of SIGN-silver obtained using the relation $\chi_2=(1.74+0.284i)\chi_3$; they are measured from the SHG experiments of gold and silver surfaces with no nanospheres. The experimental results listed in Table II are also plotted in the figure. The $|A^{2\omega}|$ values of SIGN-silver are considerably larger than those of SIGN-gold. The experimental results do not agree with the calculated values because nanospheres are partially aggregated and the effective nanospheres for the SHG enhancement are less than the coverage.

In order to investigate the SHG response in detail, we divided the SIGN above gold into three parts: the surface of the upper hemisphere (part I, $A_{\mathrm{I}}^{2\omega}$) of the nanosphere, the surface of the lower hemisphere (part II, $A_{\mathrm{II}}^{2\omega}$), and the surface of the substrate (part III, $A_{\mathrm{III}}^{2\omega}$), as shown in the inset of Fig. 8(a). We also calculated the enhancement factor in each case. Figure 8(a) shows the absolute values of $A_{\mathrm{I}}^{2\omega}$, $A_{\mathrm{II}}^{2\omega}$, and $A_{\mathrm{III}}^{2\omega}$ indicated by solid, broken, and dotted lines, respectively, as a function of the gap distance ratio d/R; Fig. 8(b) shows their phases. The values of $|A_{\mathrm{II}}^{2\omega}|$ and $|A_{\mathrm{III}}^{2\omega}|$ are close and increase sharply with a decrease in the gap distance d, whereas $|A_{\mathrm{II}}^{2\omega}|$ is considerably smaller than the other two. Since $A_{\mathrm{II}}^{2\omega}$ and $A_{\mathrm{III}}^{2\omega}$ are out of phase, they interfere destructively. This implies that the SHG light generated in the nanogap is small despite the large enhancement factors. Figures 8(c) and 8(d) show the absolute values and phases of $A_{\mathrm{I}}^{2\omega}$ and $A_{\mathrm{II}}^{2\omega}+A_{\mathrm{III}}^{2\omega}$, respectively. The absolute values are close and remain almost constant over the gap distance from 0.05 to 0.25. The factors of $A_{\mathrm{I}}^{2\omega}$ and $A_{\mathrm{II}}^{2\omega}+A_{\mathrm{III}}^{2\omega}$ are out of phase for the large gap distance. As the gap distance decreases, the phase difference between $A_{\mathrm{I}}^{2\omega}$ and $A_{\mathrm{II}}^{2\omega}+A_{\mathrm{III}}^{2\omega}$ decreases considerably, thereby resulting in a sharp increase in the SHG.

Finally, in Fig. 9, we show the calculated enhancement factors of SIGN-gold as a function of the fundamental wavelength ω for $d/R=1/10$. The spectrum comprises two structures: one at approximately 1400 nm and the other at 600 nm. The former is due to the resonance of SHG light to the second LPR band in the RA spectra at 700 nm and the latter is due to the resonance of fundamental light to the second band. The resonance structure corresponding to the first band at 530 nm observed in the RA spectra is absent

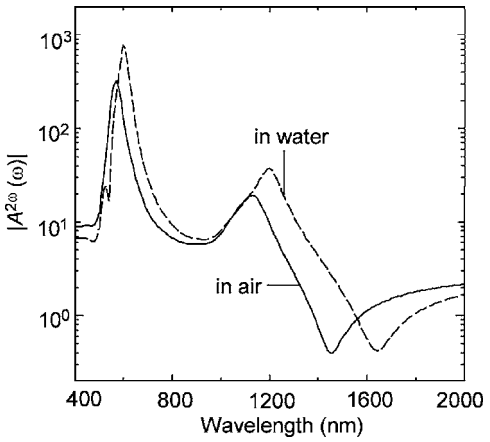

FIG. 9. Calculated field enhancement factor at $d/R=1/10$ plotted as a function of the fundamental wavelength for the SIGN-gold systems in air and water.

because of the centrosymmetric character of this band. The calculated results are consistent with those of the experimental study on the frequency dispersion of SHG in SIGN systems, which were performed with a frequency-tunable laser system.[36]

V. CONCLUSION

The linear and nonlinear optical properties of SIGNs above gold and silver surfaces were studied by considering gap distances ranging from 0.5 to 2.0 nm. A redshifted band is observed due to the multipolar interaction of the gold nanospheres with their images produced in the metallic substrate. The amount of redshift increases with a decrease in the gap distance. The wavelength at which the redshifted band of SIGNs-gold is observed is greater than that at which the redshifted band of SIGNs-silver is observed; this is in good agreement with the theoretical calculation. Moreover, we observed a significant enhancement in the SHG light from the SIGN systems at a fundamental wavelength of 1064 nm. In the SIGN-gold system, the field enhancement factor was greater than 10, while in the SIGN-silver system, it was less than 3. The former values are roughly in agreement with the calculated results of the SIGN-gold systems; however, the latter values are not in agreement probably due to the poor quality of the samples. A further detailed calculation for the SIGN-gold system shows that the SHG from the nanogap is not dominant even under the LPR condition because the nanogap region is almost centrosymmetrical. The enhanced SHG field in the SIGN system originates from the combination of the SHG fields from the upper-hemisphere surface and gap region.

ACKNOWLEDGMENTS

We thank Takayuki Okamoto (RIKEN Institute, Wako, Japan) and Kazuma Tsuboi (JST, Japan) for their helpful discussions. We also thank Masayuki Shimojo (Saitama Institute of Technology, Saitama, Japan) and Kazuo Furuya (NIMS, Tsukuba, Japan) for providing transmission electron microscope images. This study was partly supported by a Grant-in-Aid from the Ministry of Education, Culture, Sports, Science and Technology of Japan.

*Author to whom correspondence should be addressed.

[1] *Near-Field Optics and Surface Plasmon Polaritons*, edited by S. Kawata (Springer, Berlin, 2001).
[2] *Optical Properties of Nanostructured Random Media*, edited by V. M. Shalaev (Springer, Berlin, 2002).
[3] *Nano-Optics*, edited by S. Kawata, M. Ohtsu, and M. Irie (Springer, Berlin, 2002).
[4] C. F. Bohren and D. R. Huffman, *Absorption and Scattering of Light by Small Particles* (Wiley, New York, 1983), p. 130.
[5] K.-H. Su, Q.-H. Wei, Z. Zhang, J. J. Mock, D. R. Smith, and S. Schultz, Nano Lett. **3**, 1087 (2003).
[6] W. Rechberger, A. Hohenau, A. Leitner, J. R. Krenn, B. Lamprecht, and F. R. Aussenegg, Opt. Commun. **220**, 137 (2003).
[7] S. Nie and S. R. Emory, Science **275**, 1102 (1997).
[8] K. Kneipp, Y. Wang, H. Kneipp, L. T. Perelman, I. Itzkan, R. R. Dasari, and M. S. Feld, Phys. Rev. Lett. **78**, 1667 (1997).
[9] M. Futamata, Y. Maruyama, and M. Ishikawa, J. Phys. Chem. B **107**, 7607 (2003).
[10] P. K. Aravind and H. Metiu, Surf. Sci. **124**, 506 (1983).
[11] R. Ruppin, Surf. Sci. **127**, 108 (1983).
[12] M. M. Wind, J. Vlieger, and D. Bedeaux, Physica A **141**, 33 (1987).
[13] T. Kume, S. Hayashi, and K. Yamamoto, Phys. Rev. B **55**, 4774 (1997).
[14] T. Okamoto and I. Yamaguchi, J. Phys. Chem. B **107**, 10321 (2003).
[15] B. Knoll and F. Keilmann, Nature (London) **399**, 134 (1999).
[16] S. Ekgasit, F. Yu, and W. Knoll, Sens. Actuators B **104**, 294 (2005).
[17] Y. Inoue and S. Kawata, Opt. Lett. **19**, 159 (1994).
[18] H. F. Hamann, A. Gallagher, and D. J. Nesbitt, Appl. Phys. Lett. **76**, 378 (2000).
[19] E. J. Sanchez, L. Novotny, and X. S. Xie, Phys. Rev. Lett. **82**, 4014 (1999).
[20] Y. R. Shen, Nature (London) **337**, 519 (1989).
[21] N. Bloembergen, R. K. Chang, S. S. Jha, and C. H. Lee, Phys. Rev. **174**, 813 (1968).
[22] J. E. Sipe, V. C. Y. So, M. Fukui, and G. I. Stegeman, Solid State Commun. **34**, 523 (1980).
[23] R. Naraoka, H. Okawa, K. Hashimoto, and K. Kajikawa, Opt. Commun. **248**, 249 (2005).
[24] J. I. Dadap, J. Shan, K. B. Eisenthal, and T. F. Heinz, Phys. Rev. Lett. **83**, 4045 (1999).
[25] J. Nappa, G. Revillod, I. Russier-Antoine, E. Benichou, C. Jonin, and P. F. Brevet, Phys. Rev. B **71**, 165407 (2005).
[26] K. Mitsui, Y. Handa, and K. Kajikawa, Appl. Phys. Lett. **85**, 4231 (2004).
[27] K. Kemniz, K. Bhattacharyya, H. M. Hicks, G. R. Pinto, K. B. Eisenthal, and T. F. Heinz, Chem. Phys. Lett. **131**, 285 (1986).
[28] G. Berkovic and E. Shvartsberg, Appl. Phys. B: Photophys. Laser Chem. **53**, 333 (1991).
[29] K. Kajikawa, T. Yamada, S. Yokoyama, S. Okada, H. Matsuda, H. Nakanishi, M. Kakimoto, Y. Imai, H. Takezoe, and A. Fukuda, Langmuir **12**, 580 (1996).
[30] G. Decher, B. Tieke, C. Bosshard, and P. Guenter, J. Chem. Soc., Chem. Commun. 933 (1989).
[31] K. Kajikawa, M. Sei, I. Yoshida, S. Okada, H. Nakanishi, K. Seki, and Y. Ouchi, Jpn. J. Appl. Phys., Part 1 **38**, 6721 (1999).
[32] J. Y. Hang and A. Lewis, Biophys. J. **55**, 835 (1989).
[33] Y. Sotokawa, H. Okawa, K. Hashimoto, and K. Kajikawa (unpublished).
[34] P. B. Johnson and R. W. Cristy, Phys. Rev. B **6**, 4370 (1972).
[35] V. Mizrahi and J. E. Sipe, J. Opt. Soc. Am. B **5**, 660 (1988).
[36] K. Tsuboi and K. Kajikawa (unpublished).